Fuel 309 (2022) 122039

Contents lists available at ScienceDirect

Fuel

journal homepage: www.elsevier.com/locate/fuel

Full length article

Molecular dynamic simulation of the impact of thermal maturity and reservoir temperature on the contact angle and wettability of kerogen

Archana Jagadisan, Zoya Heidari *

The University of Texas at Austin, 200 E. Dean Keeton, Stop C0300, Austin, TX 78712, United States of America

ARTICLE INFO

Keywords:
Wettability
Molecular dynamics simulations
Kerogen wettability
Organic-rich mudrocks
Unconventional reservoirs

ABSTRACT

Understanding the interfacial interactions between fluids (oil and water) and kerogen is imperative for efficient development and production of hydrocarbons in unconventional shale reservoirs. Kerogen is one of the major constituents (up to 30 vol%) of organic-rich mudrocks. Thus, wettability of kerogen can directly affect the multi-phase fluid-flow properties, water production, and resistivity of organic-rich mudrocks. The chemical composition of kerogen varies with kerogen type and thermal maturity. Reservoir temperature is another factor that can have an impact on thermodynamic processes such as interfacial interactions. Therefore, it is important to fundamentally understand the impact of kerogen geochemistry and reservoir conditions on the wettability of kerogen at the molecular-scale domain. The objectives of this paper are to quantify the impacts of reservoir temperature as well as kerogen molecular structure on the three-phase air/water/kerogen and methane/water/kerogen contact angle on the kerogen surface using molecular dynamics (MD) simulations.

The MD simulations are performed on kerogen molecules of types I, II, and III at different thermal maturity levels and at a temperature range from 300 to 360 K. Simulation results showed that the air/water/kerogen contact angle formed on kerogen surface is highest for type III kerogen at 45.5° and lowest for type II kerogen at 20°. For type II kerogen, the contact angle increases from 20° to 75.5° as the thermal maturity increases from immature stage to over-matured stage. Increase in temperature from 300 to 380 K decreases the contact angle measurements by 62%. The methane/water/kerogen contact angle showed similar trend with type III kerogen having the highest contact angle (58°) among the three kerogen types. The impact of thermal maturity on methane/water/kerogen contact angle shows an increase from 25.5° to 88.5° from kerogen II-A to kerogen II-D, which is consistent with the observations from air/water/kerogen contact angles. The documented results and workflows can potentially contribute to improving formation evaluation of organic-rich mudrocks by providing information about wettability of kerogen. The outcomes of this paper can also potentially enhance the understanding the role of organic content and its geochemical properties in fluid-flow mechanisms, which can be used to predict water production in organic-rich mudrocks.

1. Introduction

Kerogen is an organic macromolecular polymer which is the main organic component of source rocks . The thermal evolution transforms the chemical structure of kerogen with increase in aromatic carbon content [1,2]. Kerogen structure condenses to mainly graphitic structure with mainly aromatic units of sp2 hybridized carbons at very high thermal maturities[3]. Different types of kerogen have variable relative abundance of hydrogen, carbon, and oxygen content. Type I kerogen is predominantly derived from marine organic matter such as phytoplankton, zooplankton and lipid-rich biomolecules. Therefore, type I kerogen is hydrogen-rich and oxygen-poor (atomic H/C of approximately 1.5, O/C of less than 0.1). Type II kerogen has intermediate hydrogen and oxygen compositions and is formed by a mixture of higher plants or marine phytoplankton. Type III kerogen is formed predominantly by terrestrial organic matter and is oxygen-rich and poor in hydrogen (H/C of less than 1.0 and O/C of approximately 0.3). Type IV kerogen is derived from charcoal or fungal bodies and hydrogen-poor and oxygen-rich similar to Type III kerogen [4]. For each type of kerogen, H/C, O/C, and aliphatic carbon content decreases with increasing thermal maturity [5].

Due to difference in chemical structure and composition between different types of kerogen and geochemical changes due to thermal maturity, the wettability of kerogen could also change with kerogen type and thermal maturity [6,7]. Alterations of wettability in conventional

* Corresponding author.
E-mail address: zoya@utexas.edu (Z. Heidari).

https://doi.org/10.1016/j.fuel.2021.122039
Received 28 May 2021; Received in revised form 15 September 2021; Accepted 16 September 2021
Available online 8 October 2021

reservoirs at higher temperatures during thermal recovery processes have been observed, leading to a shift toward water-wet at elevated temperatures [8–11]. Published research also provides evidence for impact of temperature on kerogen–oil interaction. Impact of temperature on density distribution of octane molecules on kerogen slit modeled as a graphene surface showed that there was a 2% reduction in the number of adsorbed octane molecules at higher temperatures of 393 K as compared to low temperature of 333 K [12]. Furthermore, linear relationships between temperature and the number of oil compounds confined in the kerogen slit has also been estimated using MD simulations [13]. Therefore, it is important to understand the impact of temperature on kerogen wettability.

In a recent study, Jagadisan and Heidari (2019) [7] experimentally demonstrated that kerogen wettability varies significantly with thermal maturity and that it could be water-wet at low thermal maturities. However, these experiments could not capture wettability of kerogen and organic-rich mudrocks in different kerogen types and reservoir temperature conditions. In another study, the water adsorption capacities of kerogen were found to vary with changes in temperature conditions using molecular dynamics simulations [14]. Nonetheless, the water adsorption capacities obtained from simulation could not be compared directly with the experimentally measured wettability.

Molecular dynamics simulation is considered an effective method to simulate and understand atomic level interactions for multi-scale systems [15–18]. MD simulation has been used to simulate contact angles on mineral and metal surfaces by water [19–21] and the simulated contact angles were found to be consistent with the experimental values. Another study used MD simulation techniques for obtaining three phase water/decane/silica system [22] with good success. These studies provide information on the interaction between fluid molecules and solid surfaces and the dynamic properties of interfacial water/oil at the atomic level. Molecular dynamics simulations [6,23] on kerogen wettability used a simplified kerogen model, which is composed of graphene sheets to represent kerogen. To simulate different thermal maturity levels of kerogen, variable amounts of carbonyl (C=O) functional groups was embedded on the graphene sheets. Wettability studies by simulating a water drop on kerogen surface showed that kerogen is water-wet at low thermal maturity and hydrophobic at high thermal maturity [24]. However, this study does not capture the complexity of kerogen molecular structure. Moreover, the impact of different kerogen types and temperature conditions are not taken into account.

To understand the effect of thermal maturity, kerogen type and reservoir temperature on wettability of kerogen, we investigate the three-phase contact angle of water on kerogen surfaces by employing MD simulations. Realistic molecular models of kerogen [25] for different kerogen types and at various thermal maturity levels were used for the contact angle experiments. We then quantify the impacts of kerogen type, thermal maturity, and reservoir temperature on the contact angle of a two-phase water wettability and three-phase water/methane wettability on kerogen surface using MD simulations. We then cross validate wettability results from modeling with previously published experimental results.

2. Method

Molecular models for kerogen developed by Ungerer et al. (2015) [25] are used as inputs for simulations. The structure and composition of these kerogen molecules are verified against the elemental analysis and functional data from XPS and ^{13}C NMR corresponding to the samples, documented by Keleman et al. (2007) [26]. We first condense kerogen molecular model units to form a flat kerogen surface. To study the air/water/kerogen contact angle, a water droplet is then placed on the flat kerogen surface and the contact angle is simulated on each kerogen surface, and at temperature values ranging from 300 K to 360 K. Air is represented as vacuum in these simulations. To study the methane/water/kerogen wettability on kerogen surface, the water droplet is placed on the flat kerogen surface surrounded by methane molecules and the MD simulation is performed on water and methane molecules on each kerogen surface. The contact angle for all cases is then calculated at equilibrium. We use LAMMPS (large-scale atomic/molecular massively parallel simulator) [27] to perform the molecular dynamics simulations.

2.1. Molecular models for kerogen

Fig. 1 shows the molecular models of kerogen used in this study. Simulations are performed for three types of kerogen, Type I (Kerogen I-A), Type II (Kerogen IIA), and Type IIII (Kerogen IIIA). Type I kerogen is indicative of organic matter deposited in lacustrine environment under anoxic conditions. Type II kerogen is indicative of oil-prone organic matter deposited in anoxic marine environment and finally, Type III kerogen is indicative of organic matter originating from higher plant material [25]. Furthermore, for Type II kerogen, four different thermal maturities are considered for simulations. These kerogen samples are named II-A, II-B, II-C, and II-D, where the thermal maturity increases from sample II-A to II-D.

2.2. Preparation of the kerogen surface

The construction of a flat kerogen surface is essential for the wettability assessment using sessile drop contact angle simulation because of the irregular features of the kerogen molecules. For constructing a flat kerogen surface, we use idealized walls to construct flat kerogen surface. First, 20 kerogen molecules were randomly placed in the simulation box of size $10 * 10 * 10\ nm^3$. Then, we use idealized walls with Lennard-Jones 12/6 potential [28]. The walls are placed on the two sides of the kerogen molecule along the Z-axis direction, with a fixed wall on the top and a moving wall at the bottom of the molecules.

The molecules are then condensed in Z-axis direction till the density reaches 1.1–1.35 g/cc which is the density of pure kerogen [29,30]. Subsequently, dynamics simulation in number (N), volume (V), and temperature (T) ensemble, with a Nosé thermostat at a temperature of 298 K for 200 ps to relax and equilibrate the kerogen layer. Fig. 2 shows the steps to obtain a molecular model unit of condensed kerogen type II-A. The consistent-valence forcefield (CVFF) [31] is used for kerogen molecules to perform MD simulations.

2.3. Air/water/kerogen contact angle simulation

A droplet of water consisting of 1728 water molecules with a density of 1g/cc is placed as close as possible on the flat surface of the condensed kerogen structure. We adopted the CVFF force field kerogen molecules for the simulations, which is widely used for organic molecules. The simple point charge extended (SPC/E) model is used to describe water [32]. The model is chosen since it is widely adopted and Vega et al. (2005) [33] verified the accuracy of the SPC/E-model predictions of density and water structural properties against experimental observations. The electrostatic potential and van der Waals (vdW) potential represent the nonbonding interactions. Lennard-Jones 12/6 electrostatic potential [28] is used to perform the vdW interaction. The simulations are performed using NVT ensemble and the temperature of the system is varied from 300 to 370 K, respectively. Each simulation was performed for 800 ps. The initial 600 ps is used to reach equilibrium. The remaining 200 ps of the simulation time is used to get the MD trajectory data, which is used to calculate the contact angle. Fig. 3 shows the workflow used in this paper to determine the wettability of kerogen.

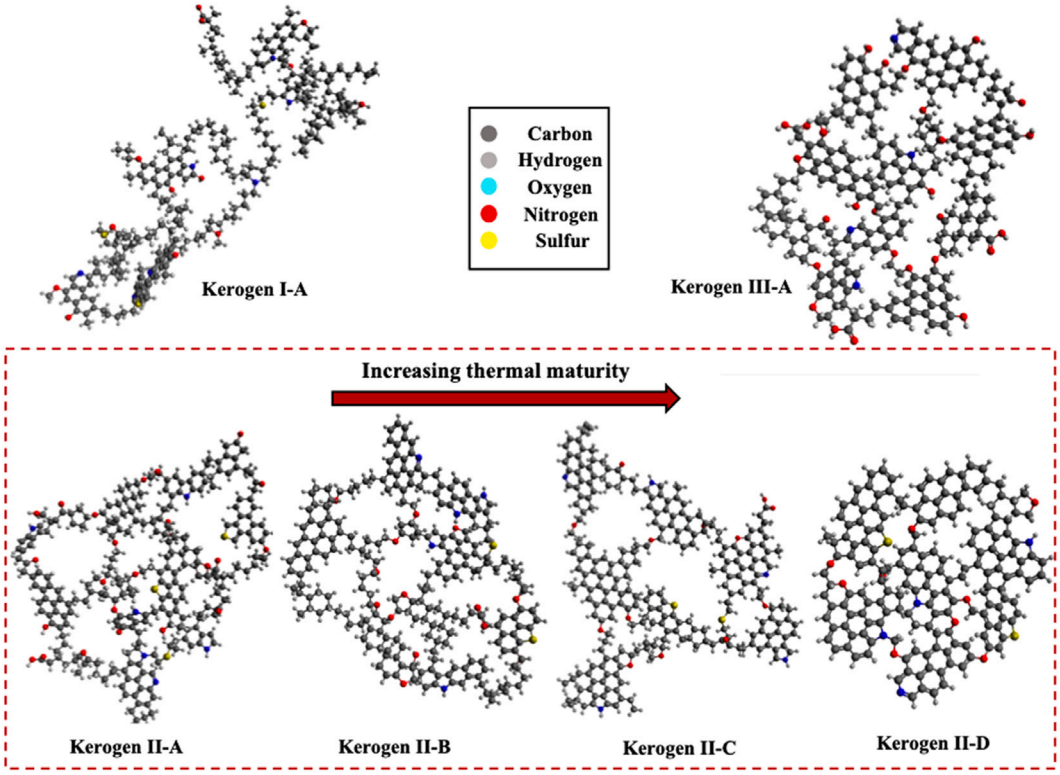

Fig. 1. Molecular model units of kerogen molecules used in this paper documented by [25].

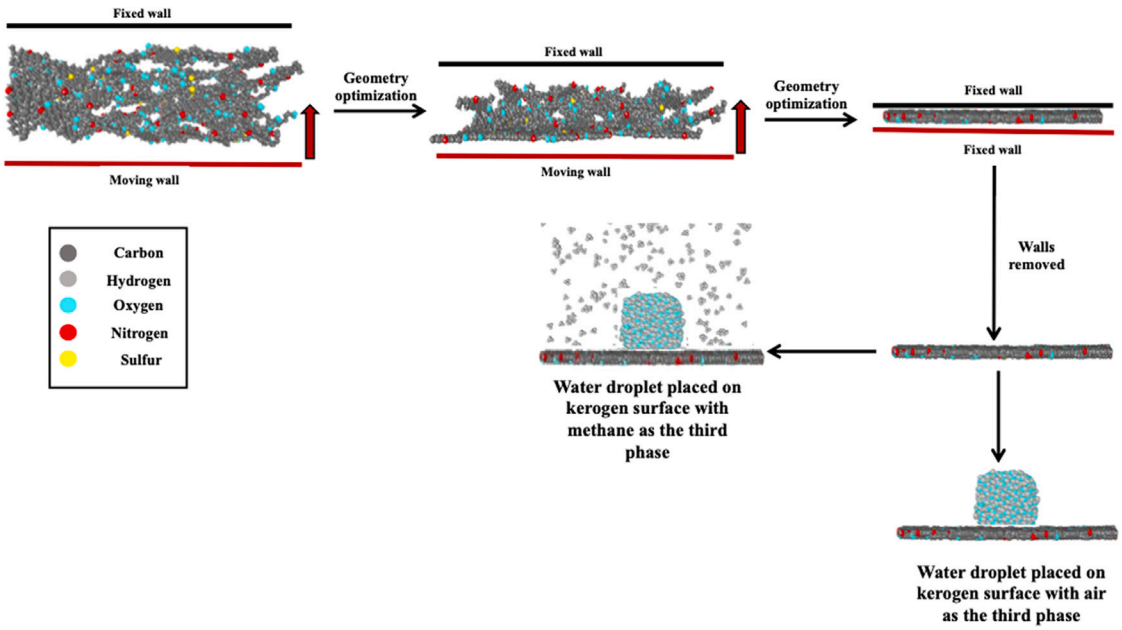

Fig. 2. The proposed workflow to construct a flat kerogen surface.

2.4. Methane/water/kerogen contact angle simulation

A droplet of water is placed on the flat surface of the condensed kerogen structure. The water droplet is then surrounded by methane molecules. Fig. 1 shows the arrangement of water and methane molecules on the top of the flat kerogen structure. The number of water and methane molecules are determined by the sizes of the cubes and the water and methane densities under the condition of 300 K and 1 bar. The arrangement of molecules and the simulations are implemented using the platform of LAMMPS. Then, NVT simulations are performed in on the fluid molecules to calculate the contact angle between water and kerogen using similar procedure described for air/water/kerogen contact angle.

2.5. Calculation of contact angle

The wettability of the kerogen surface is characterized by the contact angle formed by water droplet. The contact angle is obtained based

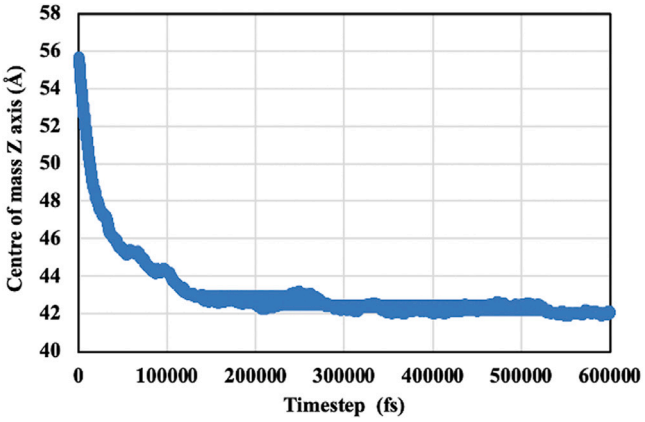

Fig. 3. An example of variation of center of mass (COM) of the water droplet in the z-axis as a function of simulation time for kerogen sample Kerogen-IIC.

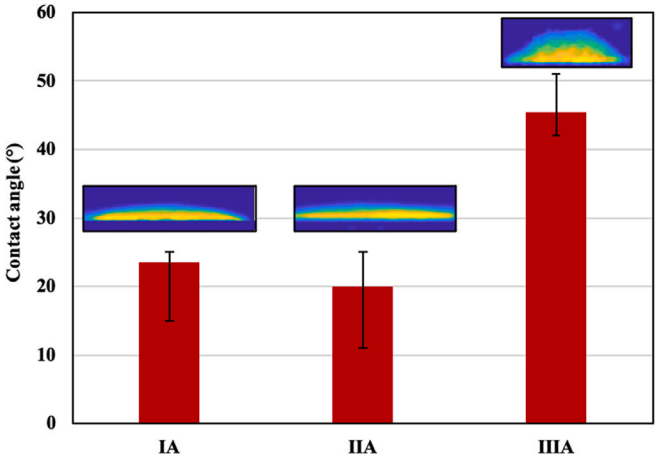

Fig. 5. Contact angle of water droplet of type I, type II, and type III kerogen, respectively.

on the density distributions of water molecules on kerogen surface. The water droplet evolves from initial configuration of cube to a semi-cylinder form and reaches to an equilibrium state. The equilibration is performed for 600 ps, which is verified by the time variation of the mass center of water droplets. At equilibrium the coordinate of the mass center has little variation (less than 2%) in the z-direction. Fig. 3 shows an example of variation of center of mass of the water droplet in the z-direction. We then simulate the system for an addition 200 ps and obtain the density distributions of the water droplets. By averaging the density distributions over 200 ps the 2D contour in the x–z plane of the density distributions is obtained. Finally, we fit a circle on the resultant density profile and calculate the contact angle of the water droplets. Fig. 4 shows the workflow used to estimate the contact angle of the air/water/kerogen and methane/water/kerogen droplet.

3. Results and discussion

3.1. Composition of kerogen molecules

Table 1 shows the composition of the kerogen molecules documented in this paper. The composition data indicates that between type I, type II, and type III kerogen of comparable thermal maturity, the O/C ratio is the lowest for type I kerogen (0.052), followed by type II kerogen (0.095), and the highest for type III kerogen (0.116). Aromaticity also follows a similar trend and is highest for type III kerogen (57%) followed by type II (41%) and type I kerogen (29%). The impact of thermal maturity in type II kerogen can be seen with decrease in O/C ratio from 0.095 to 0.051 and increase in aromaticity from 41% to 79% between Kerogen II-A to Kerogen II-D, respectively.

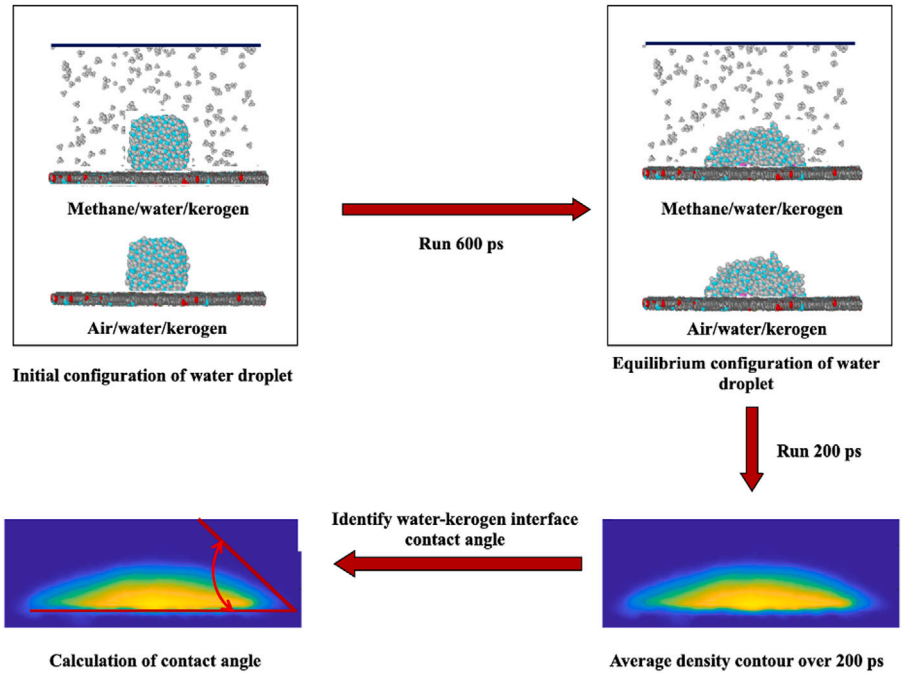

Fig. 4. The proposed workflow to obtain contact angle formed by a water droplet on kerogen surface.

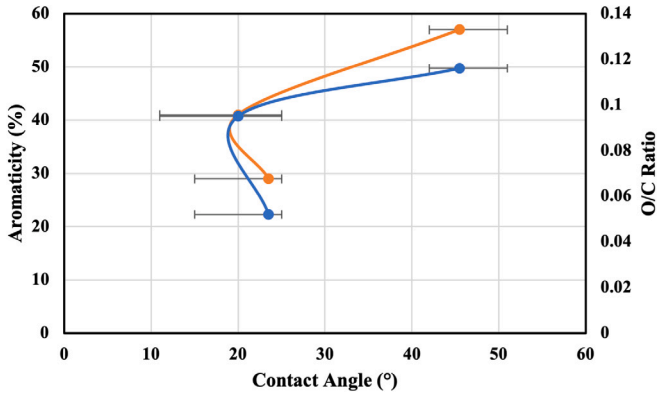

Fig. 6. Contact angle variation in kerogen type I, II and III as a function of O/C ratio and aromaticity.

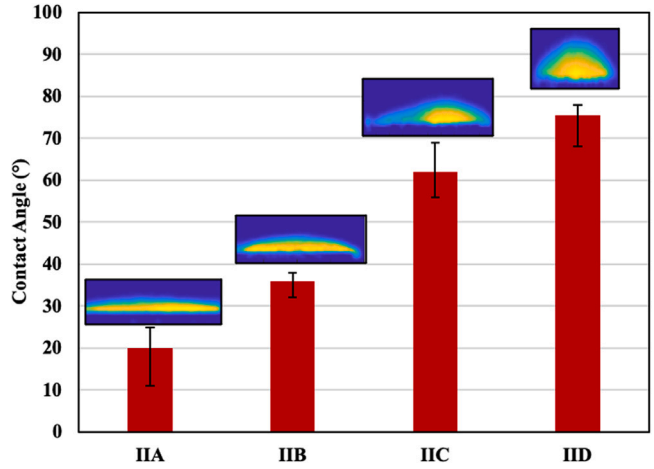

Fig. 7. Estimates of contact angle obtained using MD simulations at equilibrium state in kerogen type II at four different thermal maturities.

Table 1
Composition of kerogen molecular models. The reported data is adopted from the work published by Ungerer et al. (2015) [25].

Sample	Composition		
	H/C (Per 100 C)	O/C (Per 100 C)	Aromaticity
Kerogen I-A	1.53	0.052	29%
Kerogen II-A	1.17	0.095	41%
Kerogen II-B	1.12	0.060	45%
Kerogen II-C	0.905	0.054	58.7%
Kerogen II-D	0.58	0.051	79%
Kerogen III-A	0.886	0.116	57%

3.2. Air/water/kerogen wettability

3.2.1. Impact of kerogen type on air/water/kerogen wettability

Water droplet was simulated on the surface of three types of kerogen, Kerogen I-A, Kerogen II-A, and Kerogen III-A with the third phase being air. Fig. 5 shows the histogram of contact angle of water droplet on the kerogen surface for Kerogen I-A, Kerogen II-A, and Kerogen III-A. The results show that the contact angle measured for Kerogen I-A, Kerogen II-A, and Kerogen III-A are 23.5°, 20° and 45.5°, respectively.

Fig. 6 shows the variation of contact angle of Kerogen I-A, Kerogen II-A, and Kerogen III-A as a function of O/C ratio and aromaticity. The decrease in contact angle from 23.5° in Kerogen I-A to 20° in Kerogen II-A could potentially be because of increase in O/C ratio from 0.052 to 0.095 (Table 1) in Kerogen I-A and Kerogen II-A, respectively. However, in Kerogen III-A, the contact angle is higher at 45.5° compared to

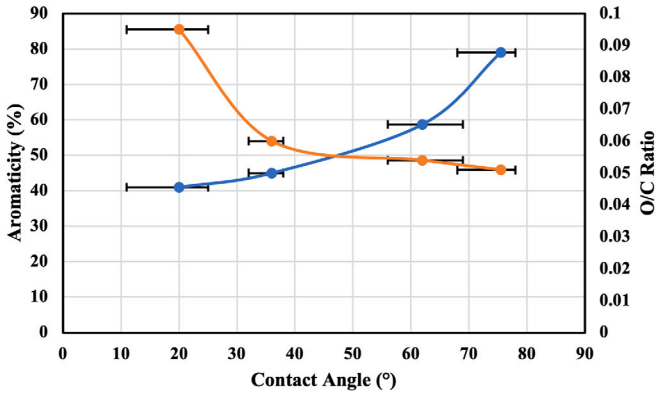

Fig. 8. Estimates of contact angle variation in kerogen type II as a function of O/C ratio and aromaticity.

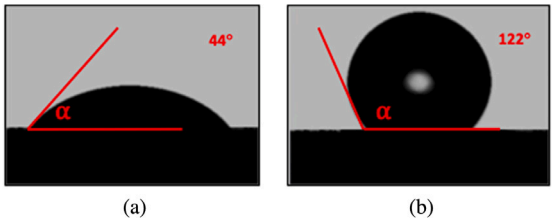

Fig. 9. Experimental results of contact angle formed by a water droplet on the surface of kerogen samples: (a) low thermal maturity kerogen sample and (b) high thermal maturity kerogen sample.

Kerogen I-A and II-A. We observe this behavior in Kerogen III-A even though the O/C (0.116) is higher than Kerogen I-A and II-A. This could potentially be due to the increase in aromaticity to 57% as compared to 29% and 41% in Kerogens I-A and II-A, respectively. This shows that contact angle is impacted by both oxygen content and aromaticity.

3.2.2. Impact of thermal maturity on air/water/kerogen wettability

Fig. 7 shows the MD simulation results of contact angle formed by a water droplet on type II kerogen surface of increasing thermal maturity A, B, C, and D, respectively. Comparisons of contact angle formed by a water droplet on kerogen samples II-A, II-B, II-C, and II-D shows that the contact angle increases from Kerogen II-A to Kerogen II-D. The contact angle is lowest at 20° for Kerogen II-A, which is at the lowest thermal maturity among the four samples.

The contact angle increases to 36°, 62°, and 75.5° for kerogen samples II-B, II-C, and II-D, respectively. This observation indicates that the water-wettability of Kerogen II-A is the highest and the wettability decreases with increasing thermal maturity and becomes hydrophobic for Kerogen II-C and Kerogen II-D.

Fig. 8 shows the variation of contact angle in type II kerogen as a function of O/C ratio and aromaticity. The results show that progressive decrease in O/C ratio from 0.095 to 0.051 and aromaticity increase from 41% to 79% between samples Kerogen II-A to Kerogen II-D results in increase in contact angle from 20° to 75.5°. This can be explained by the increase in non-polar aromatic hydrocarbons composed of non-polar C–C and C-H bonds that are insoluble in water.

3.2.3. Validation of MD results with experimental results on isolated kerogen samples

We verify the contact angle results obtained from MD simulation using sessile drop test on type II kerogen samples which are isolated from an organic-rich mudrock formation. The samples are synthetically matured by heat-treating them under controlled conditions. Figs. 9(a) and 9(b) show the contact angle obtained for kerogen samples which

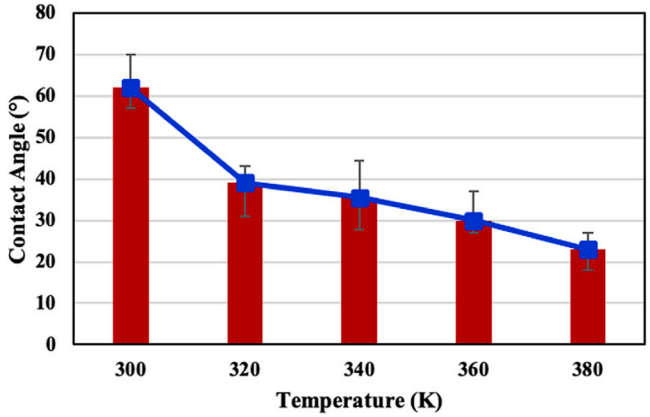

Fig. 10. Contact angle of water droplet on type I kerogen surface at 300 K, 320 K, 340 K, and 360 K, respectively.

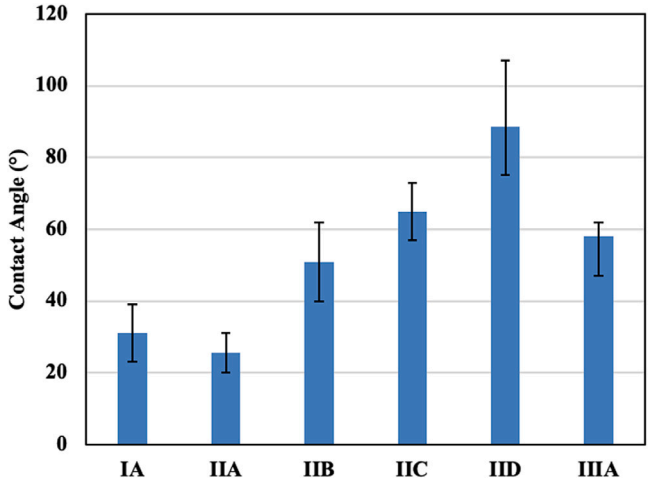

Fig. 11. Contact angle of water droplet on kerogen surface with methane as the third phase.

are at low and high thermal maturities, respectively. The results suggest that the kerogen sample at low thermal maturity has a low contact angle of 44°, indicating a hydrophilic kerogen. As the thermal maturity increases, the contact angle, formed by water droplet on kerogen surface, increases to 122°, indicating a hydrophobic kerogen. The experimental results suggest that kerogen is water-wet at low thermal maturity becomes less water-wet at high thermal maturity, which is consistent with the results obtained from MD simulations.

3.2.4. Impact of temperature on wettability of kerogen

Fig. 10 shows the MD simulation results of contact angle formed by water droplet on type II-C kerogen surface at temperatures 300, 320, 340, 360 K, and 380 K. The results show that as temperature increases, the contact angle formed by water droplet decreases. The contact angle decreases from 62° to 39° as the temperature increases from 300 K to 320 K. The contact angle further decreases to 35.5° as the temperature increases to 340 K. Finally, from 360 K to 380 K, the contact angle decreases from 30° to 23°. The results can be explained by the decrease in surface tension of the kerogen surface with increase in temperature, which results in decrease in contact angle.

3.3. Methane–water–kerogen wettability

3.3.1. Impact of kerogen type and thermal maturity on methane/water/kerogen wettability of kerogen

Water droplet surrounded by methane was simulated on the surface of three types of kerogen, Kerogen I-A, Kerogen II-A, and Kerogen III-A. Fig. 11 shows the MD simulation results of contact angle formed by a water droplet on kerogen surface at initial and equilibrium state after 800 ps, respectively. The results show that the contact angle measured for Kerogen I-A, Kerogen II-A, and Kerogen III-A are 31°, 25.5° and 58°, respectively. The results also show that contact angle of water droplet increases from 25.5°–51° with increase in thermal maturity from Kerogen II-A (H/C — 1.17, aromaticity — 41%) to Kerogen II-B (H/C — 1.12, aromaticity — 45%). It further increases from 51°–65°–88.5° with increase in thermal maturity from Kerogen II-B to Kerogen II-C (H/C — 0.905, aromaticity — 58.7%) to Kerogen II-D (H/C — 0.58, aromaticity — 79%). This shows that the water wettability in the presence of hydrocarbon kerogen decreases with increase in thermal maturity which is a similar trend with air/water/kerogen wettability.

3.4. Comparison between air/water/kerogen wettability and methane/water/kerogen wettability of kerogen

Fig. 12 compares the contact angles between air/water/kerogen and methane/water kerogen. The results show that the contact angle formed by water droplet on the surface of kerogen with air as the third phase is consistently lower than when the third phase is methane.

3.4.1. Discussion

The wettability of kerogen can depend on a number of factors including surface roughness and reservoir pressure. Moreover, the contact angle measurements in larger scales can also be influenced by the surface area of kerogen samples, the size of water droplet, surface heterogeneity, location of water droplet, to name a few. Therefore, a single parameter of kerogen geochemistry cannot accurately describe the wettability of kerogen. However, the focus of this paper is to study the relative impact of kerogen geochemistry on the contact angle and wettability of kerogen, assuming every other parameter remain the same. Thus, the outcomes of this paper in the molecular-scale can provide knowledge regarding how variation of geochemistry and thermal maturity can be used to predict changes in wettability of a given formation.

Wettability of kerogen impacts the fluid distributions as well as interactions with fracturing fluid. The exact phenomenon of how fracturing fluids interact with the kerogen pores is an area of active research. In addition to wettability of organic matter, the amount of clay present in the formation, volumetric concentration and distribution of minerals in the rock, fracturing fluid composition and geochemistry, and pore sizes could have an impact on the fracturing fluid and rock interactions. Therefore, rock–fluid interactions in organic-rich mudrocks are a complex problem that needs to be investigated in the future both numerically and experimentally.

4. Conclusions

Flat kerogen surface was created for kerogen of type I, II, and II and for four thermal maturity levels of kerogen type II. The density of the kerogen structures was maintained between 1.1 – 1.35 g/cc which was in agreement with the experimentally measured kerogen density.The results for contact angle measurements indicate a water-wet to mixed-wet nature of kerogen surfaces, with kerogen at lower thermal maturity showing a higher water wettability.

The contact angle formed by a water droplet on flat kerogen surface was then simulated using MD simulation and was analyzed after reaching equilibrium. The simulated contact angle results showed that type III kerogen (Kerogen III-A) had the highest contact angle of 45.5°

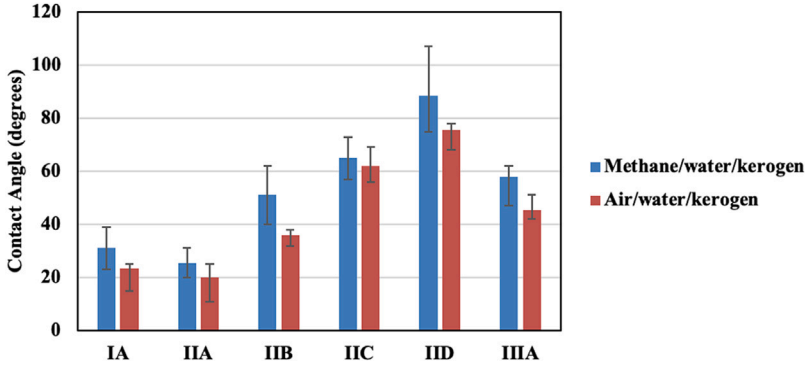

Fig. 12. Comparison of air/water/kerogen and methane/water/kerogen contact angle.

between the three types of kerogen. Type II kerogen (Kerogen II-A) had the smallest contact angle at 20°. This shows that type II kerogen could be more water-wet and type III kerogen is the least water-wet among the three different kerogen types.

The simulated air/water/kerogen contact angle formed by a water droplet on type II kerogen surface of different thermal maturity showed that increase in thermal maturity results in increase in contact angle. Kerogen II-C and Kerogen II-D had equilibrium contact angles of 62° and 75.5°, which confirms that these samples were hydrophobic. Whereas Kerogen II-A and II-B had contact angles of 20° and 36°, which indicate hydrophilic nature of these samples. The simultaneous relative decrease in O/C ratio from 0.095 to 0.051 (i.e., a decrease by 46%) and change in aromaticity from 41% to 79% (i.e., an increase of 92%) from Kerogen II-A to Kerogen II-D is potentially the main reason behind the decrease in water-wettability with increase in thermal maturity. The MD simulation results are qualitatively verified against experimental results for contact angle on isolated kerogen samples, which also shows that the contact angle increases from 44° to 122° with increase in thermal maturity. The contact angle estimates demonstrate that kerogen is strongly hydrophobic at high thermal maturities and water-wet at low thermal maturity.

The estimated contact angle results from MD simulations of water droplet on kerogen samples of type I kerogen at different temperature conditions showed that the contact angle decreases with increase in temperature from 300 K to 380 K. The results demonstrated that increase in reservoir temperature from 300 K to 360 K could result in 62% decrease in contact angle from 62° to 23°. The results demonstrate that at reservoir conditions, with increase in reservoir temperature, the water-wettability of kerogen samples increases.

The methane/water/kerogen contact angle showed similar trend as the air/water/kerogen contact angle with contact angles increasing from 25.5° to 88.5° with increase in thermal maturity from kerogen II-A to kerogen II-D. Kerogen types also showed that type III-A kerogen had the highest contact angle at 58° and type II-A kerogen had the lowest contact angle at 25.5°. The contact angles of water droplet measured with the third phase being methane was higher by approximately 20% on average, as compared to contact angle with air as the third phase.

The reported wettability of kerogen for different types, thermal maturities and temperatures can contribute to improved understanding of factors affecting wettability of organic matter and consequently wettability of organic-rich mudrocks. Performing such measurements of contact angle at reservoir temperature is extremely challenging in the laboratory. For that reason, most of the previously reported data was at laboratory temperature, which was not representative of the in-situ conditions. The documented results can improve the prediction of wettability of kerogen, provided the chemical composition and structure is known, or with information about type and thermal maturity of kerogen present in the organic-rich mudrocks. This can potentially impact formation evaluation in these rocks. Moreover, the outcomes of this paper can also potentially contribute to increased understanding of the role of organic content and its geochemical properties on fluid-flow mechanisms, which can be used to predict water production in organic-rich mudrocks.

CRediT authorship contribution statement

Archana Jagadisan: Computational work, Validation, Methodology, Formal analysis, Writing. **Zoya Heidari:** Conceptualization, Methodology, Writing, Supervision, Project administration, Funding acquisition.

Declaration of competing interest

The authors declare that they have no known competing financial interests or personal relationships that could have appeared to influence the work reported in this paper.

Acknowledgments

The work reported in this paper was funded by the Industrial Affiliate Research Program on "Multi-Scale Rock Physics" sponsored by BHP, BP, Core Laboratories, Equinor, ExxonMobil, Occidental Petroleum, Petrobras, University Lands and Wildcat Technologies. We would like to thank Dr. Gyeong Hwang and Myungsuk Lee of the Department of Chemical Engineering at The University of Texas at Austin for their technical advice regarding molecular dynamics simulations. Part of this paper was initially presented at the 2020 Society of Petrophysicists and Well Log Analysts (SPWLA) 61th annual symposium [14]. The authors acknowledge SPWLA for the permission to publish this work in the Fuel Journal.

References

[1] Vandenbroucke M. Kerogen: from types to models of chemical structure. Oil Gas Sci Technol 2003;58(2):243–69.
[2] Baskin DK. Atomic H/C ratio of kerogen as an estimate of thermal maturity and organic matter conversion. AAPG Bull 1997;81(9):1437–50.
[3] Passey QR, Bohacs KM, Esch W, Klimentidis R, Sinha S. My source rock is now my reservoir-geologic and petrophysical characterization of shale-gas reservoirs. AAPG Search Discov Article 2012;90124.
[4] Van Krevelen DW. Coal: typology-physics-chemistry-constitution. 1993.
[5] Hunt JB, Hill PG. An inter-laboratory comparison of the electron probe microanalysis of glass geochemistry. Quat Int 1996;34:229–41.
[6] Hu Y, Devegowda D, Sigal R. A microscopic characterization of wettability in shale kerogen with varying maturity levels. J Nat Gas Sci Eng 2016;33:1078–86.
[7] Jagadisan A, Heidari Z. Experimental quantification of the effect of thermal maturity of kerogen on its wettability. SPE Reserv Eval Eng 2019;22(04):1–323.
[8] Hjelmeland O, Larrondo L. Experimental investigation of the effects of temperature, pressure, and crude oil composition on interfacial properties. SPE Reserv Eng 1986;1(04):321–8.
[9] Wang W, Gupta A. Investigation of the effect of temperature and pressure on wettability using modified pendant drop method. In: SPE annual technical conference and exhibition. Society of Petroleum Engineers; 1995.

[10] Al-Hadhrami HS, Blunt MJ. Thermally induced wettability alteration to improve oil recovery in fractured reservoirs. SPE Reserv Eval Eng 2001;4(03):179–86.
[11] Mahani H, Menezes R, Berg S, Fadili A, Nasralla R, Voskov D, et al. Insights into the impact of temperature on the wettability alteration by low salinity in carbonate rocks. Energy Fuels 2017;31(8):7839–53.
[12] Wang S, Feng Q, Javadpour F, Xia T, Li Z. Oil adsorption in shale nanopores and its effect on recoverable oil-in-place. Int J Coal Geol 2015;147:9–24.
[13] Yang Y, Liu J, Yao J, Kou J, Li Z, Wu T, et al. Adsorption behaviors of shale oil in kerogen slit by molecular simulation. Chem Eng J 2020;387:124054.
[14] Jagadisan A, Heidari Z. Impact of kerogen geochemistry and reservoir temperature on contact angle and wettability of kerogen. In: SPWLA 61st annual logging symposium. OnePetro; 2020.
[15] Yan H, Yuan S. Molecular dynamics simulation of the oil detachment process within silica nanopores. J Phys Chem C 2016;120(5):2667–74.
[16] Zhang Y-Y, Pei Q-X, Jiang J-W, Wei N, Zhang Y-W. Thermal conductivities of single-and multi-layer phosphorene: a molecular dynamics study. Nanoscale 2016;8(1):483–91.
[17] Zhao J, Yao G, Ramisetti SB, Hammond RB, Wen D. Molecular dynamics simulation of the salinity effect on the n-decane/water/vapor interfacial equilibrium. Energy Fuels 2018;32(11):11080–92.
[18] Li Y, Wang S, Wang Q. A molecular dynamics simulation study on enhancement of mechanical and tribological properties of polymer composites by introduction of graphene. Carbon 2017;111:538–45.
[19] Jin J, Miller JD, Dang LX. Molecular dynamics simulation and analysis of interfacial water at selected sulfide mineral surfaces under anaerobic conditions. Int J Miner Process 2014;128:55–67.
[20] Shi B, Dhir VK. Molecular dynamics simulation of the contact angle of liquids on solid surfaces. J Chem Phys 2009;130(3):034705.
[21] Li T, Li J, Lin H, Duan Y, Xia Y, Jiang Y, et al. Control of wettability transition and coalescence dynamics of droplets on the surface via mechanical vibration: a molecular simulation exploration. Appl Surf Sci 2019;473:393–400.
[22] Xu S, Wang J, Wu J, Liu Q, Sun C, Bai B. Oil contact angles in a water-decane-silicon dioxide system: effects of surface charge. Nanoscale Res Lett 2018;13(1):1–9.
[23] Diaz Campos M, Hobson S. A novel approach for reservoir simulation and fluid characterization of unconventional fields: Phase 1 molecular level considerations. In: Abu Dhabi international petroleum exhibition and conference. Society of Petroleum Engineers; 2014.
[24] Hu Y, Devegowda D, Striolo A, Van Phan AT, Ho TA, Civan F, et al. Microscopic dynamics of water and hydrocarbon in shale-kerogen pores of potentially mixed wettability. Spe J 2015;20(01):112–24.
[25] Ungerer P, Collell J, Yiannourakou M. Molecular modeling of the volumetric and thermodynamic properties of kerogen: Influence of organic type and maturity. Energy Fuels 2015;29(1):91–105.
[26] Kelemen S, Afeworki M, Gorbaty M, Sansone M, Kwiatek P, Walters C, et al. Direct characterization of kerogen by X-ray and solid-state 13C nuclear magnetic resonance methods. Energy Fuels 2007;21(3):1548–61.
[27] Plimpton S. Fast parallel algorithms for short-range molecular dynamics. J Comput Phys 1995;117(1):1–19.
[28] Lennard-Jones JE. On the determination of molecular fields. II. From the equation of state of gas. Proc. R. Soc. A 1924;106:463–77.
[29] Okiongbo KS, Aplin AC, Larter SR. Changes in type II kerogen density as a function of maturity: Evidence from the Kimmeridge Clay Formation. Energy Fuels 2005;19(6):2495–9.
[30] Jagadisan A, Yang A, Heidari Z. Experimental quantification of the impact of thermal maturity on kerogen density. Petrophysics 2017;58(06):603–12.
[31] Dauber-Osguthorpe P, Roberts VA, Osguthorpe DJ, Wolff J, Genest M, Hagler AT. Structure and energetics of ligand binding to proteins: Escherichia coli dihydrofolate reductase-trimethoprim, a drug-receptor system. Proteins Struct Funct Bioinform 1988;4(1):31–47.
[32] Berendsen H, Grigera J, Straatsma T. The missing term in effective pair potentials. J Phys Chem 1987;91(24):6269–71.
[33] Vega C, McBride C, Sanz E, Abascal JL. Radial distribution functions and densities for the SPC/E, TIP4P and TIP5p models for liquid water and ices I h, I c, II, III, IV, V, VI, VII, VIII, IX, XI and XII. Phys Chem Chem Phys 2005;7(7):1450–6.